Numerical Methods in Civil Engineering

Effects of Mathematical Model of MR Damper on Its Control Performance; A Nonlinear Comparative Study

Reza Karami Mohammadi*, Hadi Ghamari**

ARTICLE INFO

Article history:
Received:
May 2019.
Revised:
August 2019.
Accepted:
September 2019.

Keywords:
-MR damper
-Semi active control
-MNS model
-Bouc wen model
-LQR control
-Nonlinear instantaneous optimal control

Abstract:

In this paper, the effect of mathematical representation method of an MR damper on the performance of control algorithm is investigated. The most exact and common Maxwel Nonlinear Slider (MNS) and modified Bouc-Wen hysteretic models are employed through a nonlinear comparatve numerical study. In many of semi-active control algorithms, a mathematical modelling method is required for determinig the Magneto-Rheological (MR) damper voltage at each time instant. Using different modelling methods can lead to different voltages for the MR damper, which subsequently results in changes to the responses of the controlled structure. A three story office building steel structure is excited by seven acceleration time histories. Nonlinear instantaneous optimal control (NIOC) and linear quadratic regulator (LQR) controllers are utilized as two active-based semi-active algorithms. Results of nonlinear investigations show an obvious difference between the MNS and the modified Bouc-Wen models in the performance of control algorithms. Outputs show a higher performance for the modified Bouc-Wen model in reducing the hysteretic energy in the structure.

1. Introduction

Vibration control of structures intends to preserve the vibration behaviour of a structure within a desired range. There are several types of motion control for a structure. In a performance viewpoint, there are three control categories: Active, passive, and semi-active manners. Passive control devices generate control force using the local response of the installation location. Characteristics of passive devices are not changeable. Active control devices generate control forces using an external source of electric power based on a pre-defined control algorithm. However, there is a deficiency: the drawback of this category is that, external power supply may disconnect during severe earthquakes. Also, the energy which is applied to the structure by active devices may lead to instability.

**Associate Professor, School of Civil and Environmental Engineering, K. N. Toosi University of Technology, Tehran, Iran.*
*** Corresponding Author: Ph.D. Candidate, School of Civil and Environmental Engineering, K. N. Toosi University of Technology, Tehran, Iran. E-mail: hghamari@mail.kntu.ac.ir*

On the other side, this control type is adaptable. Semi-active control devices produce control forces utilizing the local response of the installation location of device. Nevertheless, a semi-active device can change its characteristics during the excitation using a relatively small power supply e.g., a few batteries. Therefore, this system enjoys the positive features of both active and passive vibration control systems, namely, adaptability and stability, [1, 2, 3, 4].

There are numerous semi-active control devices such as Magneto-rheological (MR) dampers, Electro-rheological (ER) dampers, variable orifice devices, variable stiffness devices, etc. Among of all the semi-active devices, MR fluid based dampers are the most applicable type due to their valuable characteristics. MR damper includes micron-sized polarizable particles. These particles are dispersed in a carrier medium such as mineral or silicone oil (see Fig.1). MR fluid can change from a linear Newtonian fluid to a nonlinear semi-solid material. This transformation occurs in milliseconds due to change in magnetic field which is imposed on the MR damper. Thus, MR damper properties can change within a very short time when its commanding voltage and magnetic field changes. In addition, MR fluid has a high capacity of energy dissipation, due to the large value of yielding stress [4]. Input voltage of MR damper is the only directly controllable parameter of this damper [5].

Therefore, one of the most important phases of the control process is voltage determination using an appropriate control algorithm.

In some of the semi-active control algorithms such as Clipped Optimal Control (COC), a desired control force is determined using a reference active control algorithm such as LQR, NIOC, H^2/LQG, etc. Consequently, an input voltage is set to achieve this reference active control force via MR damper, [6, 7, 8, 9]. In an active-based semi-active control method, the controller is mostly an optimal active controller. The calculated desired active control force is converted to voltage v for current driver and a current i for MR damper. Then, the MR damper produces a control force based on local responses of its installation position and current i. This produced force can be different from the desired control force. Hashemi et al. [10] employed the Bouc-Wen model and developed a wavelet neural network-based semi-active method, which converts the desired control force to the MR damper voltage. Hiramoto et al. [7] proposed a new semi-active control strategy based on a reference active control law. Parameters of the reference active control law were optimized to improve semi-active control performance. Reference active control law predicts desired control forces. Then, based on this predicted control force, the command signal of semi-active control device is determined. The effectiveness of this method is demonstrated through a numerical investigation on a 15-DOF structural system. Liu et el. [11] introduced a semi-active control method using MR damper. They utilized an active-based method for determining the reference control forces via LQR algorithm. This research showed the efficiency of their proposed approach, especially in mitigating the drift and acceleration responses. Zafarani and Halabian [12] developed a model-based semi-active control algorithm for MR dampers. They used a simplified Bouc-Wen model for modelling MR damper hysteretic behavior. They employed active-based semi-active control algorithms for controlling the nonlinear structures.

NIOC method can be used for controlling the nonlinear structures in active control, without the risk of instability [13]. In the active NIOC algorithm, the control law for the (k+1)'th time step is defined as follows:

$$u_{k+1} = \frac{1}{12}\eta^{-1}R^{*^{-1}}B^T\left[Pz_{k+1} + q_{k+1}\right] \tag{1}$$

Where:

$$P = -\left[\frac{1}{72}\zeta Q^* B\eta^{-1}R^{*^{-1}}B^T + I\right]^{-1} Q \tag{2}$$

$$q_{k+1} = P\left[D_k + \frac{\Delta t}{6}H\ddot{x}_{gk+1}\right] \tag{3}$$

$$Q^* = \frac{\Delta t}{\zeta}Q \quad , \quad R^* = \frac{1}{\eta\Delta t}R \tag{4}$$

$$\begin{aligned} D_k = z_k + \frac{\Delta t}{6}\Big[& f_z(z_k) + 2f_z\left(z_k + \frac{1}{2}K_1\right)... \\ & + 2f_z\left(z_k + \frac{1}{2}K_2\right) + f_z(z_k + K_3)... \\ & + 5Bu_k + 5H\ddot{x}_{gk}\Big] \end{aligned} \tag{5}$$

$$K_1 = \Delta t\ S(t_k, z_k) \tag{6}$$

$$K_2 = \Delta t\ S\left(t_{k+\frac{1}{2}}, z_k + \frac{1}{2}K_1\right) \tag{7}$$

$$K_3 = \Delta t\ S\left(t_{k+\frac{1}{2}}, z_k + \frac{1}{2}K_2\right) \tag{8}$$

$$S(t_k, z_k) = f_z(z_k) + Bu_k + H\ddot{x}_{gk} \tag{9}$$

Where $f_z(z)$ denotes the system vector:

$$\dot{z}(t) = f_z(z) + Bu(t) + H\ddot{x}_g(t) \quad , \quad z(\circ) = \circ \tag{10}$$

$$f_z(z) = \begin{bmatrix} \dot{x}(t) \\ -M^{-1}f_v(t) - M^{-1}f_x(t) \end{bmatrix} \tag{11}$$

Δt represents the time step size, B stands for a matrix which locates active control forces vector (u(t)), f_v (t) and f_x (t) denote internal force vectors, related to the velocity and displacement responses, respectively. η and ζ are scalar parameters related to R and Q weighting matrices. Q has to be a positive semi-definite matrix and R must be a positive definite matrix. If Q matrix is chosen relatively large, the response reduction has more importance than the reducing control forces. The NIOC method cost function J is formulated as follows:

$$J_{k+1} = z_{k+1}^T Q z_{k+1} + u_{k+1}^T R u_{k+1} \tag{12}$$

The NIOC algorithm is used in nonlinear structures as well as linear structures. There is more detailed discussion in Huang et. al. [13].

The LQR method uses the subsequent quadratic performance index [1]:

$$J = \int_{\circ}^{\infty}\left[z^T(t)Qz(t) + u^T(t)Ru(t)\right]dt \tag{13}$$

Notations of the Equation (13) are same as the NIOC method equations. The LQR control law is:

$$u = kz \tag{14}$$

k represents the optimal gain matrix which minimizes the performance index J subjected to constraint $\left\{\dot{z}(t) = [A]\{z(t)\} + \{H\}\ddot{x}_g(t) + [B]\{u(t)\}\right\}$. k is specified using the following equation:

$$k = -R^{-1}B^T P \tag{15}$$

P denotes the symmetric positive semi-definite solution of the algebraic Riccati equation with the zero-left side:

$$\circ = PA + A^T P + Q - PBR^{-1}BP \quad (16)$$

More discussions are available in Fuller et al. [1].

A mathematical representation is mostly required for converting a reference control force to input voltage of MR damper, especially in active-based semi-active control algorithms. Spencer et. al. [14] proposed a modified Bouc-Wen model. They investigated on a phenomenological model in comparison with three other mathematical models through a set of experimental tests. They showed that the modified Bouc-Wen model can predict the MR damper behavior more accurately than Bingham, Gamota-Filisko and classic Bouc-Wen models. Cha et. al. [5] utilized the modified Bouc-Wen model on their real-time hybrid tests. They identified modelling parameters of the modified Bouc-Wen model of a 200-kN MR damper through some experimental tests. They used this model for controlling a three story office building steel structure by employing active-based semi-active control algorithms. Chae et. al. [15] proposed Maxwell Nonlinear Slider (MNS) model for modelling MR damper and tested a 300-kN MR damper. This research utilized two other mathematical models for comparison purposes: the modified Bouc-Wen, and hyperbolic tangent models. The research showed a good accuracy for the modified Bouc-Wen model. Also, they proved there was a better conformity between the experimental results and the MNS model predictions. Winter and Swartz [16] proposed a small scale MR-fluid extraction damper for testing the small-scale structures equipped with MR dampers. They used a Bouc-Wen model for mathematical representation of the damper. Yanik and Aldemir [17] developed an integrated active and semi-active (INASA) system. They proposed an active tendon combining an MR damper for INASA system. The Bouc-Wen model was used for modelling the MR damper. The research showed the effectiveness of their proposed control system.

In previous researches the main concern of MR damper mathematical model selection was the accuracy and a better agreement between the predictions of this model and the real responses. Effects of mathematical model of MR damper on global control performance of structure are investigated in this research, whereas, no attention was paid earlier. Sapinski et al. [9] and Chae et al. [15] compared different models of MR damper considering the accuracy of modelling with respect to experimental data.

First of all, the modified Bouc-Wen, and MNS models are described. Next, the utilized reference active control algorithms are introduced. Then, the characteristics of MR dampers and structure which is used for numerical investigation are deployed. Finally, the results of semi-active control of investigated structure are presented. Both the modified Bouc-Wen and MNS models are used in this research.

2. Theoretical Background

A schematic of a 300-kN MR damper is depicted in Fig. 1. This damper, manufactured by Lord Corporation, is used here for numerical investigations. Full characteristics of this large scale MR damper and its identifying tests were deployed by Chae et. al. [15]. In subsequent sections, two of the most common models of hysteretic behaviour of an MR damper are introduced, namely: the modified Bouc-Wen, and MNS models.

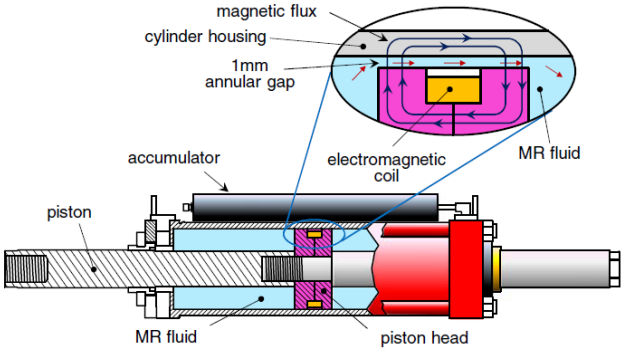

Fig. 1: Schematic of the 300-kN MR damper [15].

2.1 Modified Bouc-Wen Hysteretic Model

A phenomenological Bouc-Wen model is utilized here to model the MR damper. This model is illustrated in Fig. 2.

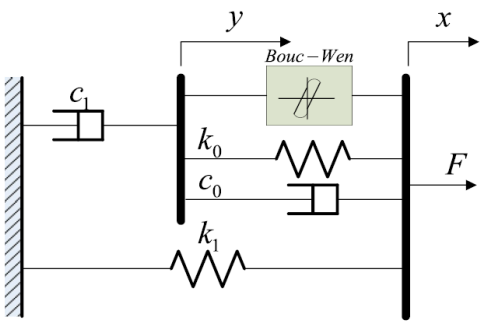

Fig. 2: Modified Bouc-Wen model [2, 3]

The modified Bouc-Wen model is formulated as follows [5]:

$$F = \alpha z + c_0(\dot{x} - \dot{y}) + k_0(x - y) + k_1(x - x_0) \quad (17)$$

$$c_1\dot{y} = \alpha z + c_0(\dot{x} - \dot{y}) + k_0(x - y) \quad (18)$$

$$\dot{z} = -\gamma|\dot{x} - \dot{y}||z|^{n-1} - \beta(\dot{x} - \dot{y})|z|^{n-1} + A(\dot{x} - \dot{y}) \quad (19)$$

Where F stands for the damper force, c_1 represents the dashpot constant for behavior of MR damper at low velocities, k_1 reveals the accumulator stiffness, c_0 and k_0 denote the damping, and stiffness values at large velocities respectively, x_0 shows the initial displacement of the spring k_1, α, β, γ, n and A are constants. These parameters have to be identified through experimental tests. The modified Bouc-Wen model was first introduced by Spencer et al. [14], and is utilized in many researches such as Sapinski et al. [9], Cha et al. [5], Chae et al. [15], etc.

2.2 Maxwell Nonlinear Slider (MNS) Model

A schematic of the MNS model is shown in Fig. 3. This model divides the response of an MR damper into two modes: pre-yield, and post-yield modes.

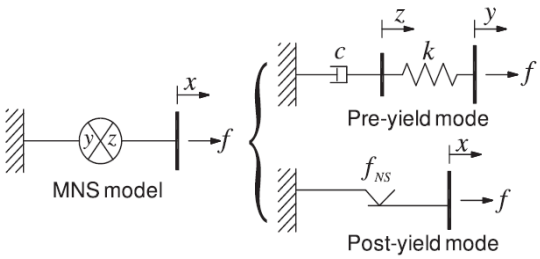

Fig. 3: MNS model [15]

Pre-yield mode is represented by a Maxwell element which includes a dashpot with coefficient c and a spring with stiffness k in series. In the pre-yield mode, the damper force f is calculated by solving the following differential equation:

$$f = k(y - z) = c\dot{z} \tag{20}$$

The responses of the pre-yield mode based on Chae et al. [15] experimental identifying tests are shown in Fig. 4. These curves were extracted at small amplitudes of harmonic loading.

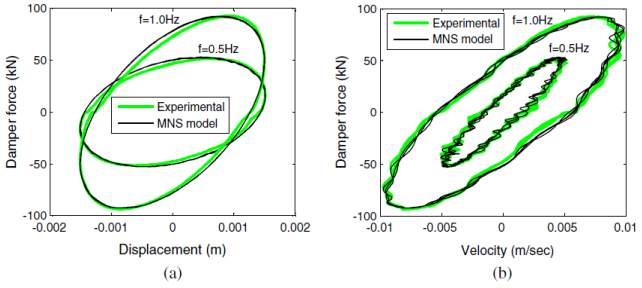

Fig. 4: Pre-yield response of MR damper based on the MNS model: a) Force-displacement response. b) Force-velocity response. [15]

Post-yield behavior can be divided into separate curves for positive and negative zones (see Fig. 5). The following equation is formulated for positive curve of the post-yield mode:

$$f_{py}^{+}(\dot{x}) = \begin{cases} a^{+} + b^{+}\left|\dot{x}\right|^{n+} & \text{if } \dot{x} \geq \dot{x}_t^{+} \\ a_t^{+}\left(\dot{x} - \dot{x}_t^{+}\right) + f_t^{+} & \text{if } \dot{x} < \dot{x}_t^{+} \end{cases} \tag{21}$$

There is a similar equation for negative curve of the post-yield mode as follows:

$$f_{py}^{-}(\dot{x}) = \begin{cases} a^{-} + b^{-}\left|\dot{x}\right|^{n-} & \text{if } \dot{x} \leq \dot{x}_t^{-} \\ a_t^{-}\left(\dot{x} - \dot{x}_t^{-}\right) + f_t^{-} & \text{if } \dot{x} > \dot{x}_t^{-} \end{cases} \tag{22}$$

a, b, n and $\dot{x}_t$ are parameters of the MNS.

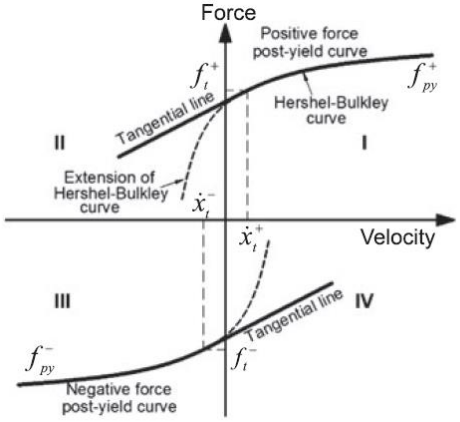

Fig. 5: Post-yield curves of the MNS model [15].

Where, $a_t^{\pm} = b^{\pm}n^{\pm}\left|\dot{x}_t^{\pm}\right|^{n^{\pm}-1}$ and $f_t^{\pm} = a^{\pm} + b^{\pm}\left|\dot{x}_t^{\pm}\right|^{n^{\pm}}$. Based on **Fig. 6,** there is a small difference between increasing and decreasing phases on the MR damper response curves. Taking this problem into account, the subsequent equation is employed:

$$f = \begin{cases} f_{py}(\dot{x}) & \text{increasing phase} \\ f_{py}(\dot{x}) + m_{\circ}(\ddot{x}) & \text{decreasing phase} \end{cases} \tag{23}$$

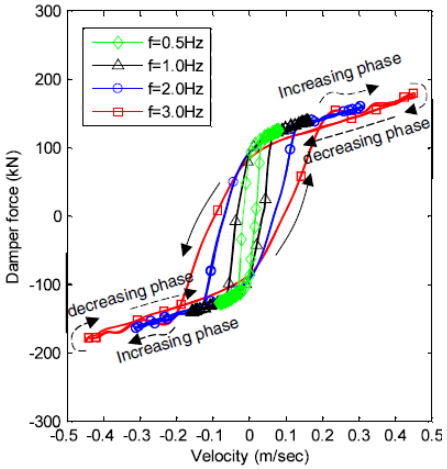

Fig. 6: Force-velocity response of MR damper based on the MNS model [15].

m_0 represents a constant. Chae et al. [15] completely introduced the MNS model in their research.

2.3 State space representation of equation of motion

Equation of motion of earthquake excited structure can be written as follows:

$$[M]\{\ddot{x}\} + [C]\{\dot{x}\} + [K]\{x\} = [M]\{l\}\ddot{x}_g(t) \tag{24}$$

[M], [C] and [K] represent the mass, damping, and stiffness matrices, respectively. x , $\dot{x}$ and $\ddot{x}$ denote the relative displacement vector, relative velocity vector, and relative

acceleration vector of the system respectively. $\ddot{x}_g$ reveals the ground acceleration. The system can be transferred into state space as follows [1]:

$$\{\dot{z}(t)\} = [A]\{z(t)\} + \{H\}\ddot{x}_g(t) \tag{25}$$

z(t) denotes the state vector of system, [A] represents the open-loop plant matrix and {H} shows a matrix for adjustment of applying point(s) of earthquake inertia force.

$$[A] = \begin{bmatrix} [o] & [I] \\ -[M]^{-1}[K] & -[M]^{-1}[C] \end{bmatrix}_{2n\times 2n} \tag{26}$$

$$\{H\} = \begin{Bmatrix} \{o\} \\ [M]^{-1}\{\delta\} \end{Bmatrix}_{2n\times 1} \tag{27}$$

{δ} adjusts applying point(s) of inertia force, n stands for the number of stories, I and o denote the identity and zero matrices respectively. δ vector is defined as follows:

$$\{\delta\} = [-m_1 \quad -m_2 \quad \dots \quad -m_n]^T_{n\times 1} \tag{28}$$

Uppercase T suggests the transpose, and m_i represents the seismic mass of the i'th story. There is an introduction to the state space formulation in Fuller et al. [1].

2.4 Semi-active control method

Two active-based semi-active control algorithms are employed here: an LQR-based method and an NIOC-based controller. The following steps describe an active-based semi-active control method:

1 – An active control law has to be designed first. (Here, the LQR or NIOC)

2 – The matrices of structural system are formed at each time step (m, c, and k matrices).

3 – Reference active control force is calculated (Using formulation of the introduction part).

4 – The reference active control force is converted to voltage of MR damper (Using the prementioned iterative procedure).

Based on previous researches such as Chae et al. [15] and Cha et al. [5], the parameters of an MR damper were always identified for some discrete values of currents. Therefore, there are only some discrete values of currents which can be chosen for a specified mathematical model (e.g. modified Bouc-Wen, MNS, etc.). In the present research, the current determination will be an iterative process during every single time step. In this state, the analysis is implemented for all possible discrete currents, and the best current is selected as the current that commanded the MR damper. It results in better control performance, but at the cost of consuming more time.

In the subsequent section, a three story office building is introduced for numerical investigations. This structure is controlled utilizing three MR dampers, each installed on a single story. Two reference active control algorithms are employed to calculate desired control forces: the LQR, and NIOC algorithms. These algorithms are used in cheap and expensive modes with different Q weighting matrices. Finally, results are presented and compared.

3. Numerical Investigations

A three story office building steel structure is employed here, where all stories have an equal area of 22500 square feet and the resulting total area is 67500 square feet. There are 6 bays in each direction with 25-ft width, and the height of all stories is 12.5-ft. This structure is shown in Fig. 7. Each of primary directions has four moment resisting frames (MRF), which are shown in blue color and four MR damper braced frames depicted in yellow color. The structure has a full symmetry in both directions. Therefore, only one-fourth of total area would be analyzed as tributary seismic area. Also, two directions will be considered independently due to symmetry principles. Cha et al. [5] used 0.6-scale model of this structure as shown in Fig. 8. Story height of the scaled model is 7.5-ft and its bay width is 15-ft. All diaphragms are supposed to be rigid. Presently, one MRF and one MR damper braced frame will be analyzed in order to analyze the whole structure.

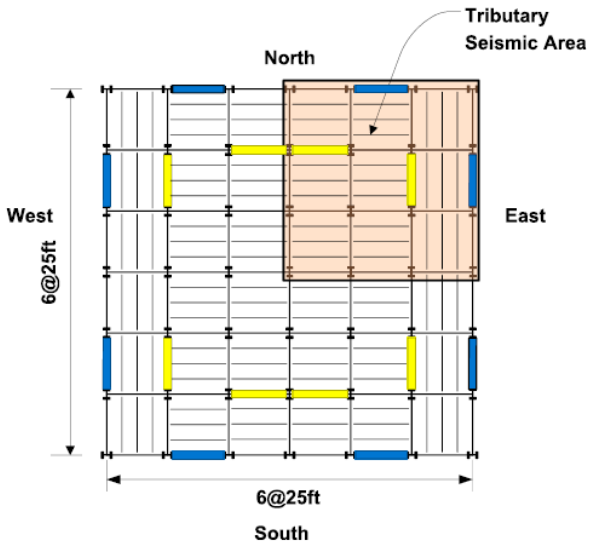

Fig. 7: Structure model

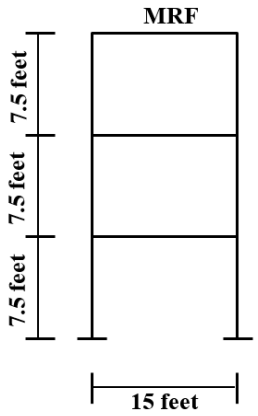

Fig. 8: 0.6 scaled MRF frame model

The vertical degrees of freedom are eliminated using the static condensation method. Then, the mass, and stiffness matrices of scaled model are extracted through finite element concepts. The damping matrix is calculated using the Rayleigh method with Five percent of critical damping for the first, and the second modes of vibration. The mass, damping, and initial stiffness matrices of the structure are presented below:

$$[m]=\begin{bmatrix} 1.020e+05 & \circ & \circ \\ \circ & 1.020e+05 & \circ \\ \circ & \circ & 7.391e+04 \end{bmatrix} \text{ kg}$$

$$[k]=\begin{bmatrix} 2.637e+08 & -2.182e+08 & 4.827e+07 \\ -2.182e+08 & 2.975e+08 & -1.244e+08 \\ 4.827e+07 & -1.244e+08 & 8.014e+07 \end{bmatrix} \text{ N / m}$$

$$[c]=\begin{bmatrix} 6.82E+05 & -5.09E+05 & 1.13E+05 \\ -5.09E+05 & 7.61E+05 & -2.90E+05 \\ 1.13E+05 & -2.90E+05 & 2.36E+05 \end{bmatrix} \text{ N.sec/ m}$$

Seven acceleration time histories are used here. Each record has a different value of PGA. Four records are scaled based on ASCE/SEI7-10 [18] and three records are originally used (unscaled). These are listed in the following Table 1. Large values of PGA, make the structure behave nonlinearly during analysis.

Table 1. Acceleration time histories

Record Name	Earthquake	Year	Station Name	PGA
SAN	San Fernando	1971	Old Ridge Root	0.32g
Elcent	Elcentro	1940	Elcentro Array 9	0.50g
NORT	Northridge	1994	Alhambra 90	0.50g
VICT	Victoria Mexico	1980	Cerro Prieto	0.63g
Tabas	Tabas	1978	Tabas	0.86g
Kobe	Kobe	1995	Kobe University	1.00g
IMP	Imperial Valley	1979	Elcentro Array	1.50g

Three 300-kN MR dampers are used here for numerical investigations. Parameters of these dampers were identified in Chae et al. [15] and used in the present paper. The parameters were given in Chae et al. [15] for the discrete values of currents: 0, 0.5, 1.0, 1.5, 2.0 and 2.5-A.

Q and R matrices of LQR-based, and NIOC-based semi-active control methods are considered as follows:

$$Q=\rho\times\begin{bmatrix} 1 & \cdots & \circ \\ \vdots & \ddots & \vdots \\ \circ & \cdots & 1 \end{bmatrix}_{6\times 6} \tag{29}$$

$$R=\begin{bmatrix} 1 & \cdots & \circ \\ \vdots & \ddots & \vdots \\ \circ & \cdots & 1 \end{bmatrix}_{3\times 3} \tag{30}$$

Coefficient of Q weighting matrix (ρ) is adjusted based on a set of pre-analysis results. When the Q is selected relatively large, reducing the responses has more importance than reducing the control forces, and vice versa. Here, the allowable values for the maximum of control forces is less than 10% of the structural seismic weight, while the control performance of the algorithm is acceptable. If Q matrix is selected relatively large, then, the maximum of control forces would be larger than the desired value. On the contrary, if Q matrix is selected relatively small, then, the control performance would not be acceptable. Therefore, an optimum value has to be chosen. Two levels of control are introduced: cheap control and expensive control. In the cheap mode of control, small value of the maximum of control forces will be achieved, and the expensive mode of control tries to achieve the best control performance with a larger value of maximum of control forces. The ρ coefficient is adjusted for different control algorithms and different control modes based on previous comments. The results are listed in Table 2.

Table 2. Coefficient of Q weighting matrix (ρ).

ρ Coefficient	cheap control	expensive control
LQR	1.0 e +10	1.0 e +11
NIOC	1.0 e +12	1.0 e +13

Three comparative criteria are introduced. The first is the drift criterion, the second criterion belongs to the hysteretic energy and the third one denotes the acceleration response criterion.

$$J_1=\left\{\frac{\max_{t,i}|\Delta_i(t)|}{\max_{t,i}|\Delta_{iU}(t)|}\right\} \tag{31}$$

$\Delta_i(t)$ represents the interstory drift of *i*'th story at time t and $\Delta_{iU}(t)$ shows the interstory drift of the uncontrolled structure at time t.

$$J_2=\left\{\frac{\max_i E_{hi}}{\max_i E_{hUi}}\right\} \tag{32}$$

E_{hi} represents the total hysteretic energy of *i*'th story and E_{hUi} stands for the total hysteretic energy of the uncontrolled structure. It should be noted that the hysteretic energy is calculated for both ends of each beam. Finally, the J_3 criterion is defined as follows:

$$J_3=\left\{\frac{\max_{t,i}|a(t)|}{\max_{t,i}|a_U(t)|}\right\} \tag{33}$$

$a(t)$ represents the response of relative acceleration of *i*'th story at time t, and $a_U(t)$ shows the relative acceleration of *i*'th story of the uncontrolled structure at time t.

UI Sim-Cor™ is implemented for analyzing the structure. This hybrid simulation code employs the OpenSees™, and Matlab™ softwares simultaneously. Implicit Newmark integration method with alpha equal to 0.25 and beta equal to 0.1667 is used.

Table 3. Results of evaluation criteria

	LQR Based		NIOC Based	
	Cheap	Expensive	Cheap	Expensive
J1				
SAN Bouc	0.8434	0.803	0.8434	0.8283
SAN MNS	0.8535	0.8131	0.8535	0.8485
Elcent Bouc	0.8738	0.7864	0.8738	0.8091
Elcent MNS	0.8576	0.7281	0.8576	0.7767
NORT Bouc	0.8857	0.7339	0.8911	0.7607
NORT MNS	0.9018	0.7268	0.9018	0.7946
VICT Bouc	0.821	0.7642	0.821	0.8122
VICT MNS	0.8559	0.8472	0.8559	0.8515
Tabas Bouc	0.8465	0.6149	0.8465	0.5916
Tabas MNS	0.8837	0.6074	0.8828	0.5805
Kobe Bouc	0.8683	0.6244	0.8683	0.8683
Kobe MNS	0.8171	0.622	0.8171	0.8341
IMP Bouc	0.9456	0.7609	0.9478	0.8956
IMP MNS	0.9565	0.75	0.9565	0.9022
Average Bouc	0.8692	0.7268	0.8703	0.7951
Average MNS	0.8752	0.7278	0.8750	0.7983
Bouc/MNS	0.9932	0.9986	0.9946	0.9960
J2				
SAN Bouc	0.1466	0.0941	0.1493	0.1344
SAN MNS	0.2111	0.1344	0.2112	0.2056
Elcent Bouc	0.7923	0.6265	0.7929	0.737
Elcent MNS	0.8324	0.6209	0.8324	0.763
NORT Bouc	0.765	0.6078	0.7667	0.5389
NORT MNS	0.809	0.6	0.8088	0.5345
VICT Bouc	0.3951	0.2839	0.3983	0.377
VICT MNS	0.5639	0.3964	0.5639	0.5503
Tabas Bouc	0.82	0.6723	0.8181	0.624
Tabas MNS	0.8717	0.6996	0.8716	0.6329
Kobe Bouc	0.8997	0.7097	0.8982	0.7679
Kobe MNS	0.8864	0.7029	0.8851	0.7771
IMP Bouc	0.8692	0.7267	0.871	0.821
IMP MNS	0.8942	0.7338	0.8943	0.8293
Average Bouc	0.6697	0.5316	0.6706	0.5714
Average MNS	0.7241	0.5554	0.7239	0.6132
Bouc/MNS	0.9249	0.9570	0.9264	0.9319
J3				
SAN Bouc	0.9298	0.9266	0.9279	0.9271
SAN MNS	0.9583	0.9571	0.9583	0.9608
Elcent Bouc	1	1.0388	0.9903	1
Elcent MNS	0.9806	1	0.9806	0.9806
NORT Bouc	0.9862	0.9811	0.9862	0.9485
NORT MNS	0.9724	0.9422	0.9724	0.9309
VICT Bouc	0.9484	0.9619	0.9484	0.9048
VICT MNS	0.9777	0.97	0.9777	0.9806
Tabas Bouc	1.0083	0.9959	1.0083	0.9244
Tabas MNS	0.9911	0.992	0.9911	0.9247
Kobe Bouc	1	0.9114	1	0.9896
Kobe MNS	0.9479	0.901	0.9479	0.9479
IMP Bouc	1.0512	1.07	1.0512	1.0419
IMP MNS	1.0465	1.0651	1.0465	1.0279
Average Bouc	0.9891	0.9837	0.9875	0.9623
Average MNS	0.9821	0.9753	0.9821	0.9648
Bouc/MNS	1.0072	1.0085	1.0055	0.9975
Control Force				
SAN Bouc	25.5	84.1	25.5	37.9
SAN MNS	20.2	85.7	20.2	35.1
Elcent Bouc	62.8	187	62.8	110
Elcent MNS	85.7	222	85.7	107
NORT Bouc	43.6	113	43.6	134
NORT MNS	47.7	110	47.7	137
VICT Bouc	28.1	89.6	28.1	34.1
VICT MNS	24	91.2	24	39.6
Tabas Bouc	56.1	171.4	56.1	209.5
Tabas MNS	70.9	165.9	70.9	209.4
Kobe Bouc	119	344	119	283
Kobe MNS	206	311	206	276
IMP Bouc	70.1	234	70.2	241
IMP MNS	108	230	108	234
Average Bouc	57.886	174.7286	57.9	149.9286
Average MNS	80.357	173.6857	80.35714	148.3
Bouc/MNS	0.7204	1.0060043	0.720533333	1.010982

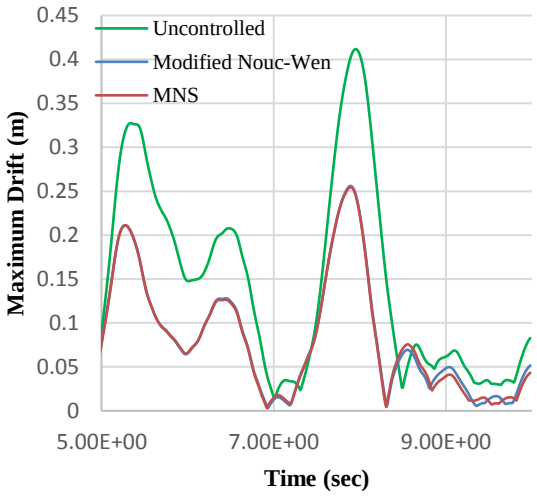

Fig. 9: Time history of the maximum of drifts (expensive mode of control of the Kobe record).

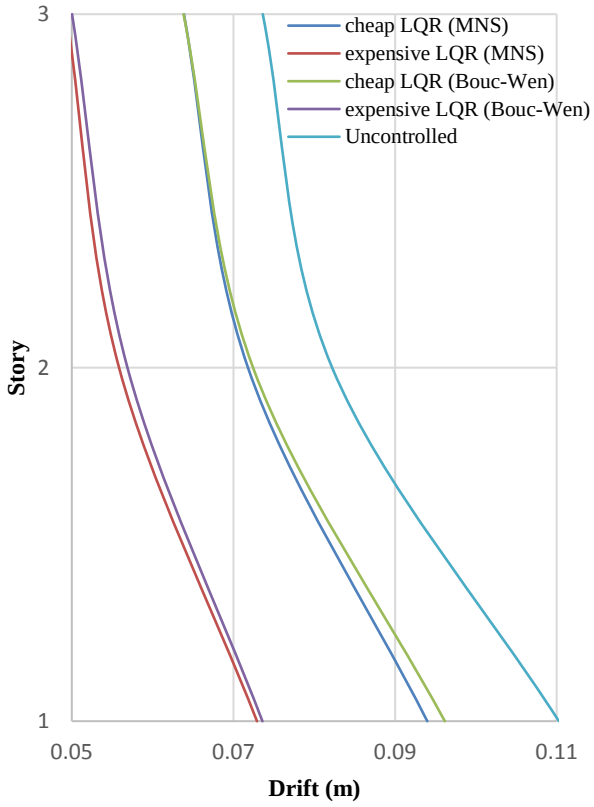

a.LQR method vs. uncontrolled

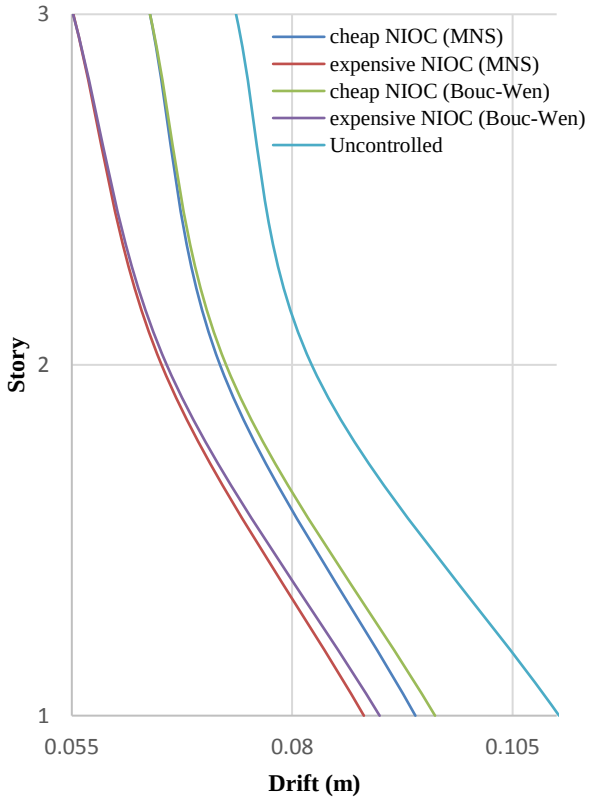

b. NIOC method vs. uncontrolled

Fig. 10: Diagram of the average of maximum story drift

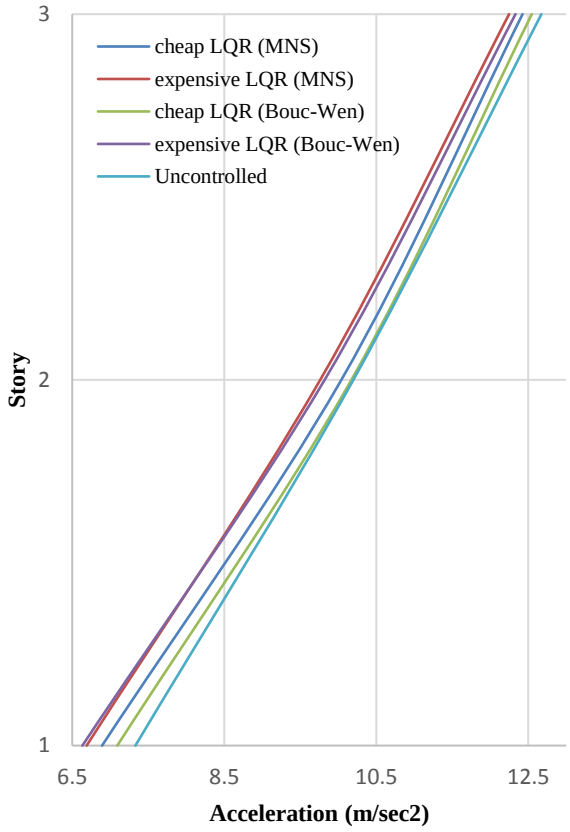

a.LQR method vs. uncontrolled

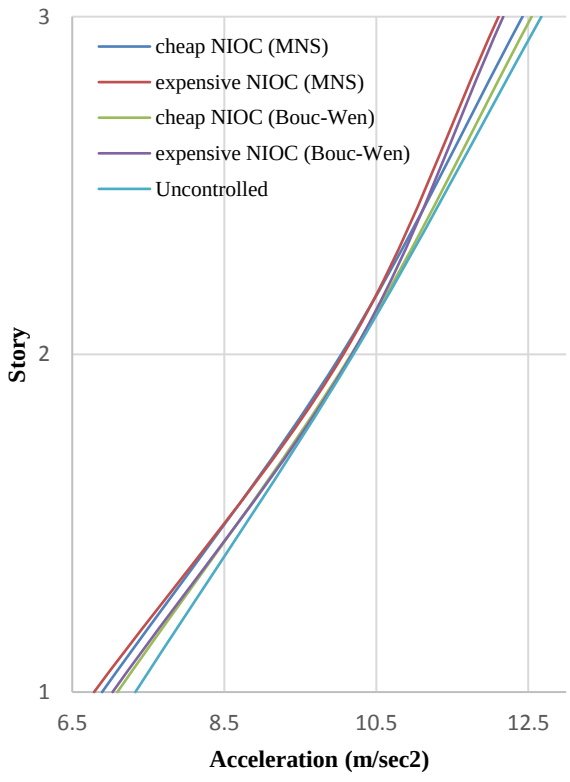

b. NIOC method vs. uncontrolled

Fig. 11: Diagram of the average of peak relative acceleration

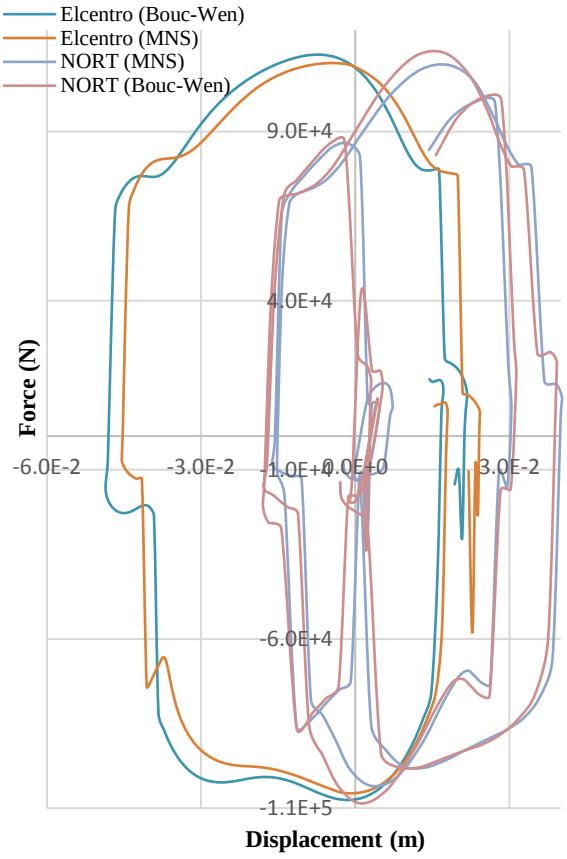

a. The 1st story

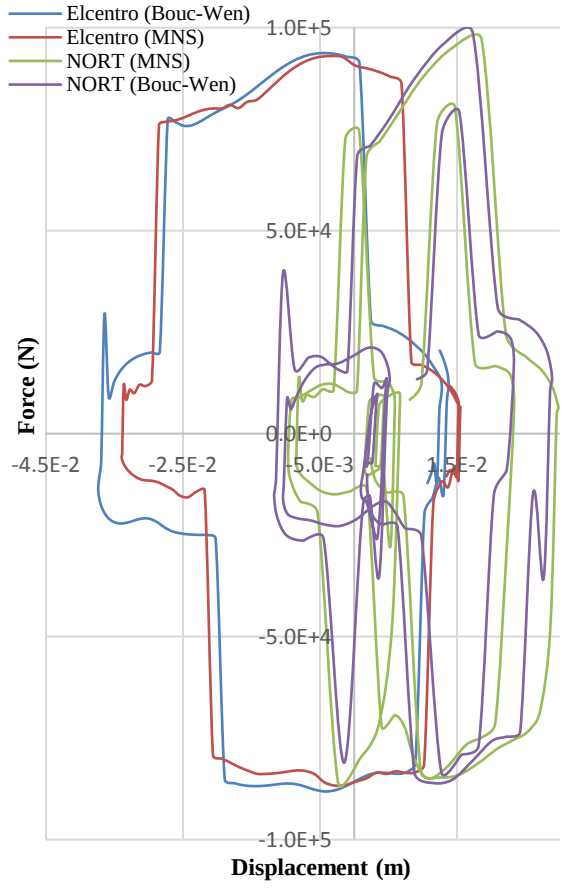

b. The 2nd story

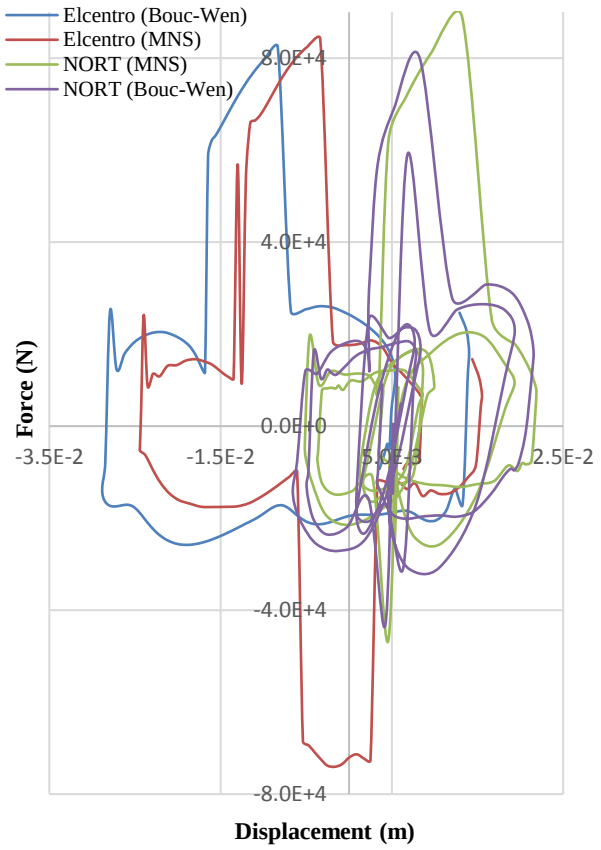

c. The 3rd story

Fig. 12: Diagram of the force – displacement of the MR dampers (control algorithm: LQR-based semi-active)

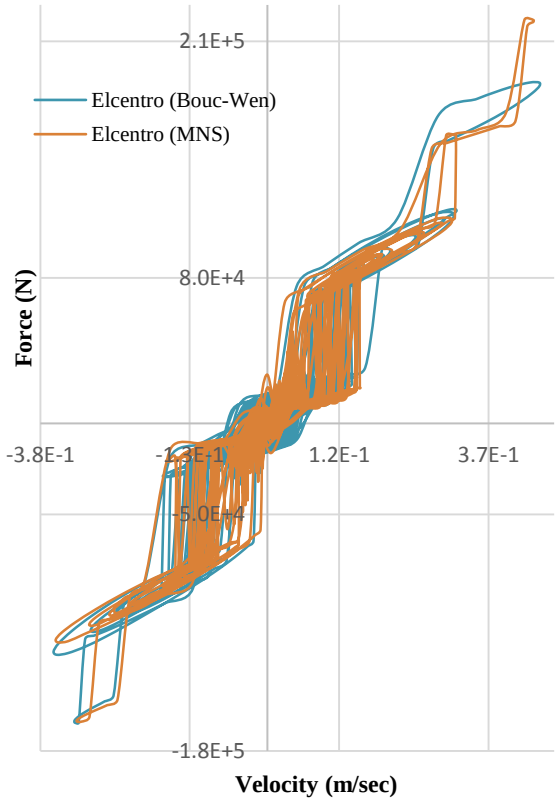

a. The 1st story

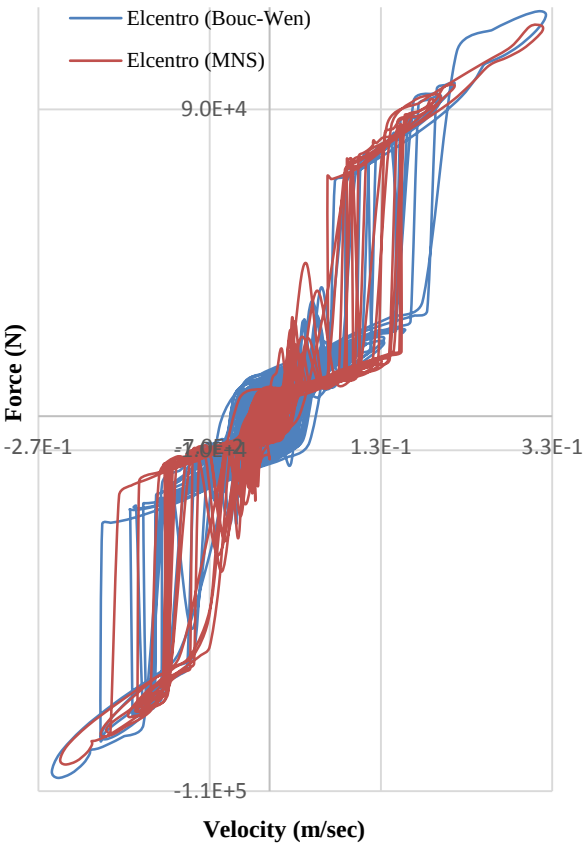

b. The 2nd story

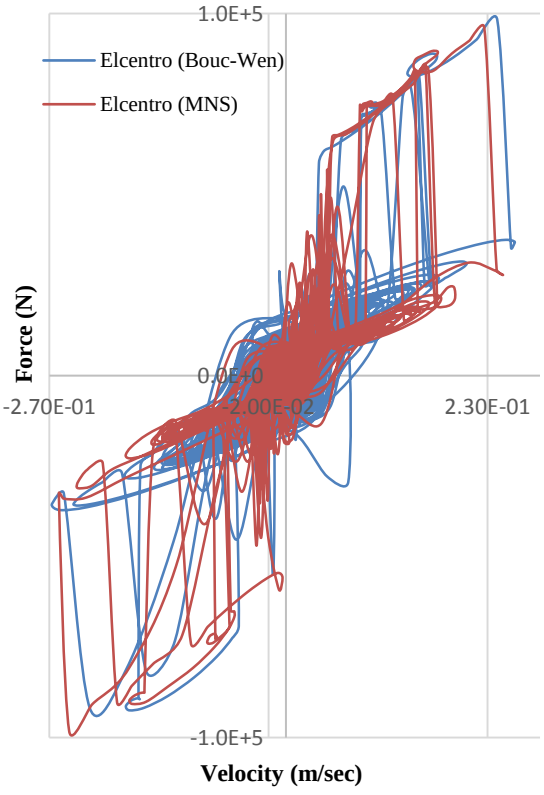

c. The 3rd story

Fig. 13: Diagram of the force – velocity of the MR dampers (control algorithm: LQR-based semi-active)

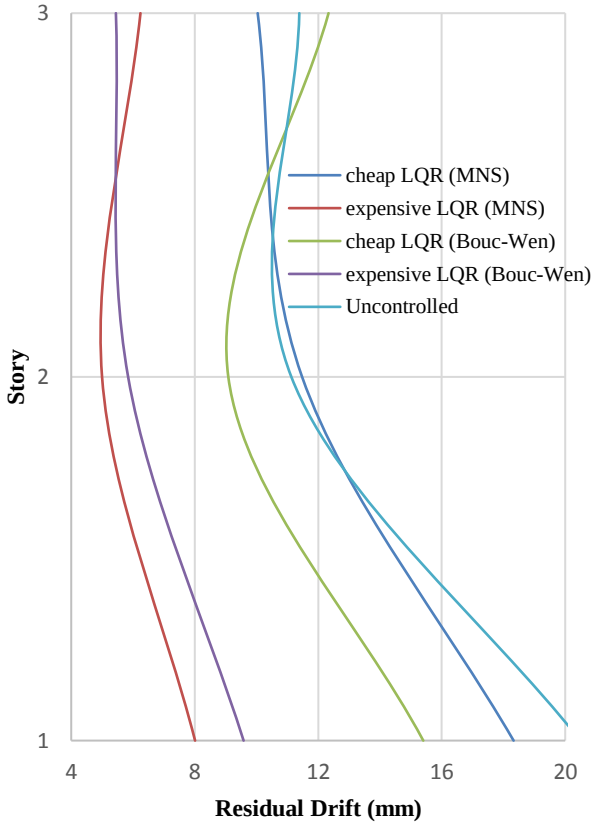

a.LQR method vs. uncontrolled

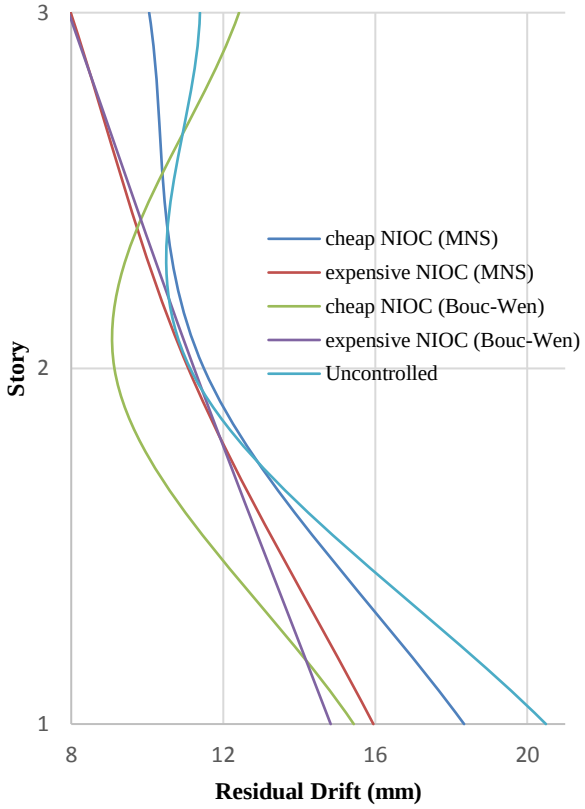

b. NIOC method vs. uncontrolled

Fig. 14: Diagram of the average of residual drifts

Results of analysis based on these three criteria and the maximum of control forces are listed in Table 3. In this table, the average values of the modified Bouc-Wen model and the MNS model are calculated for each mode of control. The ratio of average values of these two mathematical models are calculated in the Bouc/MNS rows.

Based on the results, some comments are noteworthy:

a. The modified Bouc-Wen model performs better than the MNS model in J_2 criterion. In other words, the modified Bouc-Wen model has outperformed the other model in reducing the maximum of hysteretic energy. This observation is correct for the averages of all the control algorithms, and all the control modes.
b. There is no pronounced difference between these two models in reducing the other responses, e.g. drift and acceleration responses.
c. The LQR-based semi-active control algorithm has outperformed the NIOC-based algorithm in reducing the drift response for the expensive mode of control.
d. There is no evident difference between these two algorithms for the cheap mode of control.
e. The LQR-based control algorithm has outperformed the NIOC-based algorithm in reducing the maximum of hysteretic energy for the expensive mode of control.
f. The NIOC-based control algorithm has reduced the acceleration response more than the LQR-based algorithm for the expensive mode of control.
g. Based on the J_3 criterion, the control performance of these two algorithms for the cheap mode of control is the same.
h. The maximum of required control forces for the expensive mode of control for the modified Bouc-Wen model is same as the MNS model.
i. The modified Bouc-Wen model requires a smaller capacity of MR damper for the cheap mode of control, while it performs in the same way as the MNS model in J_1, J_2, and J_3 criteria. In other words, if a designer selects a cheap control, then, the modified Bouc-Wen model would be an appropriate choice.
j. Choosing the NIOC-based algorithm for the expensive control leads to a smaller capacity of MR damper. However, the LQR-based algorithm promotes the ability of control system.
k. Fig.10 and Fig.11 display the effectiveness of all control modes and algorithms in controlling the structure in comparison with uncontrolled structure. This advantage occurs in acceleration and drift.

Fig. 9 depicts the drift response history of the first story for the cheap mode of control of the Kobe record. This figure depicts the discrepancy between the two MR damper models in a time duration of response history. Also, Fig. 10 and Fig. 11 display the maximum of drift and relative acceleration of all stories in the height of building. Fig. 12 and Fig. 13 show the force-displacement and the force-velocity histories for the modified Bouc-Wen and the MNS models, respectively. Finally, Fig. 14 displays the residual drift of all stories in the height of building. These figures prove the differences between the modified Bouc-Wen model and the MNS model in control performance of an MR damper. Fig. 14 proves the higher effectiveness of the LQR-based semi-active control algorithm for reducing the residual drifts.

It should be noted that there is no considerable difference between the two investigated models in time cost of analysis.

4. Summary and Conclusion

A comparative study on two mathematical models of MR damper has been implemented in this research: the modified Bouc-Wen model and the MNS model. These models are employed in this research through two active-based semi-active control algorithms on a nonlinear three story office building structure: an LQR based and a NIOC based semi-active control algorithms. The three 300-kN MR dampers utilized, are each installed on a story. Seven acceleration time histories with different intensities are used for numerical investigations, including very severe and severe records with PGA value of 1.0g and 1.5g. These large values of PGA, make the structure exceed the linear limit during the nonlinear analysis. For better contrast, two control modes are set: the cheap mode of control with smaller Q weighting matrix and the expensive mode of control with larger values of Q matrix.

Final results show a superiority for the modified Bouc-Wen model in reducing the hysteretic energy, while the ability of this model for reducing the maximum of drift and acceleration is similar to the MNS model.

The LQR-based algorithm, results in a higher control performance for the maximum of drifts, the maximum of hysteretic energy, and the residual drifts. Also, the NIOC-based algorithm requires a smaller capacity of MR damper. It reduces the acceleration responses more significantly than the LQR-based algorithm.

5. Discussion

Time delay probable effects on the control performance of two investigated algorithms should be studied. Also, more researches are required for evaluating the impacts of structural height on the results and conclusions. Other mathematical models of MR damper can be used for a better outcome.

References

[1] Fuller, C. R., Elliott, S. J. & Nelson, P. A., 1996. *Active Control of Vibration.* s.l.:Academic Press.

[2] Soong, T. T. & Dargush, G. F., 1997. *Passive Energy Dissipation Systems in Structural Engineering.* s.l.:John Wiley & Sons, Ltd. (UK).

[3] Connor, J. J., 2003. *Introduction to Structural Motion Control.* s.l.:Pearson Education Ltd..

[4] Cheng, Y. F., Jiang, H. & Lou, K., 2008. *SMART STRUCTURES, Innovative systems for Seismic Response Control.* s.l.:CRC Press.

[5] Cha, Y.-J.et al., 2013. Comparative Studies of Semiactive Control Strategies for MR Dampers: Pure Simulation and Real-Time Hybrid Tests. *JOURNAL OF STRUCTURAL ENGINEERING*, pp. 1237-1248.

[6] Dyke, S. J., Spencer Jr., B. F., Sain, M. K. & Carlson, J. D., 1996. *Experimental Verification of Semi-Active Structural Control Strategies Using Acceleration Feedback.* Chiba, Japan, s.n., pp. 291-296.

[7] Hiramoto, K., Matsuoka, T. & Sunakoda, K., 2016. Semi-active vibration control of structural systems based on a reference active control law: output emulation approach. *STRUCTURAL CONTROL AND HEALTH MONITORING*, Volume 23, pp. 423-445.

[8] Jansen, L. M. & Dyke, S. J., 2000. Semi-Active Control Strategies for MR Dampers: A Comparative Study. *Journal of Engineering Mechanics*, pp. 795-803.

[9] Sapinski, B. & Filus, J., 2002. ANALYSIS OF PARAMETRIC MODELS OF MR LINEAR DAMPER. *JOURNAL OF THEORETICAL AND APPLIED MECHANICS*, 41(2), pp. 215-240.

[10] Hashemi, S. M. A., Haji Kazemi, H. & Karamodin, A., 2016. Localized genetically optimized wavelet neural network for semiactive control of buildings subjected to earthquake. *STRUCTURAL CONTROL AND HEALTH MONITORING.*

[11] Liu, Y., Lin, T. & Chang, K., 2018. Analytical and experimental studies on building mass damper system with semi-active control device. *Structural Control and Health Monitoring.*

[12] Zafarani, M. M. & Halabian, A. M., 2018. Supervisory adaptive nonlinear control for seismic alleviation of inelastic asymmetric buildings equipped with MR dampers. *Engineering Structures*, Volume 176, pp. 849-858.

[13] Huang, K., Betti, R. & Ettouney, M. M., 1999. INSTANTANEOUS OPTIMAL CONTROL FOR SEISMIC ANALYSIS OF NON-LINEAR STRUCTURES. *Journal of Earthquake Engineering*, 3(1), pp. 83-106.

[14] Spencer Jr., B. F., Dyke, S. J., Sain, M. K. & Carlson, J. D., 1997. Phenomenological Model For Magnetorheological Dampers. *Journal of Engineering Mechanics*, pp. 230-238.

[15] Chae, Y., Ricles, J. M. & Sause, R., 2013. Modeling of a large-scale magneto-rheological damper for seismic hazard mitigation. Part I: Passive mode. *EARTHQUAKE ENGINEERING & STRUCTURAL DYNAMICS*, Volume 42, p. 669–685.

[16] Winter, B. D. & Swartz, R. A., 2017. Low-force magneto-rheological damper design for small-scale structural control. *Structural Control and Health Monitoring.*

[17] Yanik, A. & Aldemir, U., 2019. A simple structural control model for earthquake excited structures. *Engineering Structures*, Volume 182, pp. 79-88.

[18] American Society of Civil Engineers & Structural Engineering Institute, 2010. Minimum Design Loads for Buildings and Other Structures. *ASCE/SEI.*